Computational Study of the Oxidation and Decomposition of Dibenzofuran under Atmospheric Conditions

Mohammednoor Altarawneh, Eric M. Kennedy,* Bogdan Z. Dlugogorski, and John C. Mackie†

Process Safety and Environment Protection Research Group, School of Engineering, The University of Newcastle, Callaghan, NSW 2308, Australia

Received: January 6, 2008; Revised Manuscript Received: May 7, 2008

The atmospheric degradation of dibenzofuran (DF) initiated by OH addition has been studied by using density functional theory (B3LYP method). Site C1 in DF is predicted to be the favored site for OH addition, with a branching ratio of 0.61 to produce a DF-OH(1) adduct. The calculated reaction rate constant for OH addition to DF has been used to predict the atmospheric lifetime of DF to be 0.45 day. Three different modes of attack of O_2 ($^3\Sigma_g$) on DF-OH(1) have been examined. Abstraction of hydrogen *gem* to OH in DF-OH(1) by O_2 ($^3\Sigma_g$) (producing 1-dibenzofuranol I) and dioxygen addition in the three radical sites in *cis* and *trans* orientation (relative to the *ispo*-added OH) of the π-delocalized electron system of DF-OH(1) are feasible under atmospheric conditions. The free energy of activation (at 298.15 K) for the formation of 1-dibenzofuranol is 15.1 kcal/mol with a free energy change of −36.3 kcal/mol, while the formation of DF-OH(1)-O_2 adducts are endergonic by 9.2−21.8 kcal/mol with a 16.3−23.6 kcal/mol free energy of activation. On the basis of the calculated reaction rate constants, the formation of 1-dibenzofuranol is more important than the formation of DF-OH-O_2 adducts. The results presented here are a first attempt to gain a better understanding of the atmospheric oxidation of dioxin-like compounds on a precise molecular basis.

1. Introduction

The persistent organic pollutants (POP), polychlorinated dibenzo-*p*-dioxins, and polychlorinated dibenzofurans (PCDD/Fs) are emitted to the atmosphere from a diverse range of emission sources.[1,2] Their adverse biological effects and high toxicities[3,4] are well documented, and consequently PCDD/Fs are an important target for source reduction. Atmospheric concentrations of PCDD/Fs have been measured at various sites around the globe,[5–8] and their presence in remote locations confirms the long-range atmospheric transport (LRAT)[5] of PCDD/Fs, often a significant distance away from their original source.

The congeners of PCDD/Fs display a very wide range of liquid−vapor pressures (p_L), which dominate their long-range transport. Their p_L values range from 10^{-2} to 10^{-7} Pa, decreasing with the number increase of chlorine atoms in the parent molecule.[9] Under atmospheric conditions, PCDD/Fs are partitioned according to their p_L values, where congeners containing less than four chlorine atoms per molecule are found mainly in the gas phase. PCDD/Fs with five or six chlorine atoms per molecule are distributed between gas and solid phases, while PCDD/Fs with seven or eight chlorine atoms per molecule are predominantly found in the solid phase.[10–12] For gaseous PCDD/Fs, their depletion under atmospheric conditions occurs primarily through their reaction with OH, NO_3 radicals, and O_3.[13–15] As the reactions of PCDD/Fs compounds with NO_3 and O_3 are very slow,[15–17] the reaction with the hydroxyl radical (OH) is considered to be the major atmospheric sink for PCDD/Fs and indeed all aromatic compounds.[18] The reaction of gaseous PCDD/Fs congeners with OH was reported to be at least 8 and 3 orders of magnitude faster than their reactions with O_3 and NO_3 radicals, respectively.[15] Indeed, when considering a global mass balance for PCDD/Fs, gaseous PCDD/Fs depletion is a consequence of reaction with OH.[2]

Under atmospheric conditions, the reaction of OH with the aromatic compounds occurs primarily (approximately 90%) via addition to the benzene ring, to form a hydroxycyclohexadienyl-type radical, such as in the case for benzene,[19,20] toluene,[21,22] and *p*-xylene,[23,24] rather than through H abstraction reaction. Similarly, under atmospheric conditions, OH undergoes an addition reaction to form energized PCDD/Fs-OH adducts.[15,25] The subsequent degradation steps following the formation of the PCDD/Fs-OH adduct are not well understood. The kinetics of competition between the unimolecular transformation of initial adducts and their bimolecular reaction with other atmosphere constituents is uncertain and open to speculation. Such knowledge is of great importance in order to understand the fate of gaseous PCDD/Fs released into the atmosphere, especially their atmospheric lifetimes.

Ab initio molecular orbital electronic calculations are a widely adopted tool to help interpret experimental findings and to provide the theoretical understanding of many chemical transformation processes. Density functional theory (DFT), for example, has been used previously[25] to study mechanistically the addition of the OH radical to dibenzo-*p*-dioxin (DD), 2,3,7,8-tetrachelorodibenzo-*p*-dioxin (2,3,7,8-TCDD), and octachlorodibenzo-*p*-dioxin (OCDD). The *ipso* OH addition does not appear to be affected by chlorination patterns and takes place at the four outer carbon atoms of the benzene rings as well as at the oxygen-bonded carbon atoms.

In this work, a comprehensive first principles theoretical investigation is presented for the atmospheric oxidation of the nonchlorinated dibenzofuran (DF) by the OH radical. As the dibenzofuran moiety exists in other PCDD/Fs, the results of this study are applicable to other gaseous PCDF congeners and serve as a template and submodel for their subsequent atmospheric degradation.

* To whom correspondence should be addressed. E-mail: eric.kennedy@newcastle.edu.au. Fax: (+61 2) 4921 6920. Telephone: (+61 2) 4921 6172.
† Also at School of Chemistry, University of Sydney.

10.1021/jp800093j CCC: $40.75
Published on Web 07/09/2008

SCHEME 1: Addition of an OH Radical to Dibenzofuran (DF)

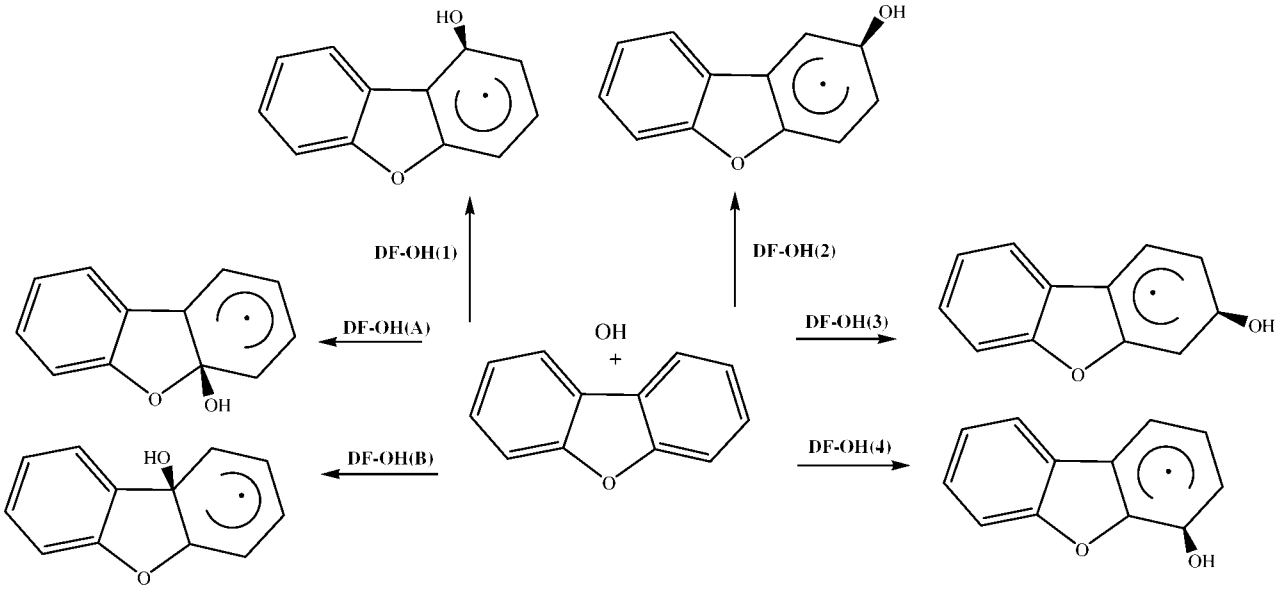

2. Theoretical Method

Electronic structures calculations have been performed using the Gaussian 03[26] suite of programs. The hybrid density functional theory (DFT) of B3LYP has been used to calculate optimized geometries and harmonic vibrational frequencies of all species and transition states on the reaction potential energy surface. This procedure deploys the exact three parameter Becke exchange functional,[27] B3, along with the Lee−Yang−Parr nonlocal correctional functional LYP[28] using the d-polarized split-valence 6-31G(d)[29] basis set. Single point calculations with the largest practical basis set of 6-311+G(3df, 2p) have been performed on the geometry obtained with the 6-31G(d) basis set. Using this computational approach, we have recently calculated the heat of formation ($\Delta_f H_{298}$ for dibenzofuran in very good agreement with the experimental value[30] which could serve as a benchmark for the accuracy of the calculated reaction energies. Diagonalization of the Hessian matrix specifies the nature of the stationary points where a transition structure contains one and only one negative eigenvalue along the reaction pathway. Intrinsic reaction coordinate calculations were performed once for each class of reactions to link reactants and products with their transition states. The high-pressure limiting rate constants for unimolecular (k_{uni}) and bimolecular reactions (k_b) were calculated using conventional transition state theory (TST).[31] Tunneling effects are accounted for using the Eckart method.[32] Reaction symmetry numbers in terms of all possible sites have been included in the rate constant calculations. Rate constant calculations have been performed using TheRate Code[33] installed at the CSEO online resource (http://www.cseo.net). Reaction rate constants can be evaluated using TheRate by deploying either the TST or the variational transition state theory (VTST). TheRate code also supports several methods to estimate the transmission coefficient.

3. Results and Discussions

Atmospheric oxidation of DF is initiated by OH addition to the benzene ring carbon atoms (C1−C4) or to the oxygen−carbon-bonded atom in the furan ring (C_A) or to the carbon−carbon-bonded atom in the furan ring (C_B) as shown in Scheme 1. These atomic labels are marked in the DF structure shown in Figure 1. The branching ratio between these six possible isomers is determined in order to locate the most stable DF-OH adducts. The formed π-delocalized DF-OH adducts react with an oxygen molecule, O_2 ($^3\Sigma_g$), either through addition to the hydroxyl-cyclohexadienyl ring to form a hydroxycyclohexadienyl peroxy radical or through H abstraction of hydrogen *gem* to OH by O_2 ($^3\Sigma_g$), affording a closed shell dibenzofuranol structure, or to the H(C) atom at the H−C−OH group to produce an oxepin-like structure on the hydroxyl-cyclohexadienyl ring. These reactions are shown in Scheme 2. For all the reactions considered, reaction energies ($\Delta_r E_0$), activation energies ($\Delta E^{\ddagger}$), reaction enthalpies ($\Delta_r H_{298}$), activation enthalpies ($\Delta H^{\ddagger}$), free energies of reactions ($\Delta_r G_{298}$), and free energies of activation ($\Delta G^{\ddagger}$) were determined based on the total energy differences between transition structures/products and these are reported in Tables 1–3. The focus of the discussion in the text is on the free energy values, which are very close to their energy and enthalpy counterparts for unimolecular reactions. For bimolecular reactions, such as OH addition to DF and O_2 reactions with DF-OH adducts, the entropy penalty resulting from species loss gives rise to the less energetically favored free energy change.

3.1. DF-OH Adducts. Optimized geometries at the B3LYP/6-31G(d) level of theory for DF-OH adducts and their corresponding transition structures are displayed in Figure 1. In the transition state structure for the formation of DF-OH(1), the adjacent C−C bonds lengthen by 0.016 Å for C1−C_B and by 0.022 Å for C1−C2, increasing to 0.100 and 0.116 Å, respectively, in DF-OH(1), characterizing a more σ-bond-type character as the electron density is transferred from the delocalized benzene ring of DF to the newly formed C−OH bond. A noticeable difference in C−O bond length is observed in TS_OH(B); it becomes shorter by 0.100 Å in comparison to the other transitional structures (TS_OH(1−4, A)). Transition vectors for TS_OH(1−4, A-B) correspond to the vertical movement of the OH group toward the carbon site. The H atom attached to the carbon atom involved in forming the bond folds back slightly to accommodate the incoming OH group.

The energetics for the addition reactions are reported in Table 1. In terms of $\Delta_r E_0$ and $\Delta_r H_{298}$ values, all adducts are stable with respect to the separated reactants. Negative values for activation energies and enthalpies are encountered for most

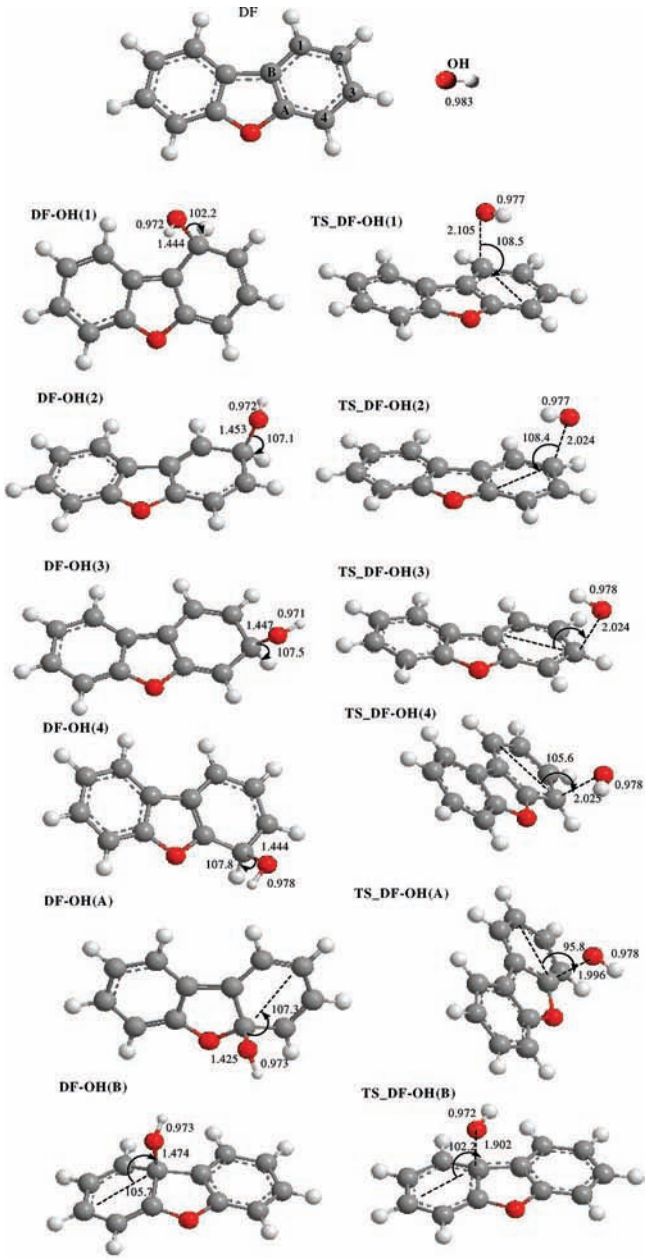

Figure 1. Optimized structures for DF-OH adducts and their corresponding transition structures (interatomic distances in angstroms, and angles in degrees).

adducts. Such a trend has been observed both theoretically[22,23,34,35] and experimentally[17,18,36,37] for OH addition to aromatic compounds including PCDD/Fs. For example, Chen et al.[35] have calculated the activation energy for OH addition to benzene theoretically and have obtained values of −1.5, −1.5, and −3.0 kcal/mol using CBS-Q//MP2(full)/6-31G(d), B3LYP/6-311+G(2df,p)//B3LYP/6-31G(d,p) [very similar to the computational approach used in this study], and CBS-Q//B3LYP//B3LYP/6-31G(d,p) methods, respectively. Our calculated value for the activation energies for OH addition to DF at sites 1, 2, and 3 reside between these values. Interestingly, the values calculated for the benzene system by Chen et al.[35] using the high-level method of CBS-Q//MP2(full)/6-31G(d) are the same as those obtained by the computational approach of B3LYP/6-311+G(2df,p)//B3LYP/6-31G(d,p) which is very similar to the computational approach used in this study. When using the high-level computational method of G3, Chen et al.[35] have obtained a positive barrier of 0.83 kcal/mol. However, this G3 value has been lowered by 1.2 kcal/mol in order for the rate constant of the addition process to match the experimental measurements. In ref 22, the negative activation energy for OH addition to different sites of toluene ranges between −3.36 and −5.00 kcal/mol using the B3LYP/6-31G method. These values become slightly positive when using the PMP2 method; however, energy contamination by the existence of the high spin state was excessive, and it strongly influenced the simulation. In a nutshell, our calculated activation barriers for OH addition to DF are in accord with those calculated for simpler aromatics using higher theoretical levels.

The negative barrier for these types of reactions is often explained[22] by the presence of a prereactive complex formed when the reactants approach each other (i.e., van der Waals complex formation). This complex is lower in energy than the separated reactants and below the transition structure. All reactions are spontaneous at 298.15 K, except for OH addition to C_B where a negative entropy change of 32 cal K^{-1} mol^{-1} results in the formation of DF-OH(B) with a Gibbs free energy change of +7.2 kcal/mol at 298 K. It is worthwhile to mention here that Lee et al.[25] have shown that the error in estimation of the Gibbs free energy due to the out-of-plane OH, ring-puckering, ring-twisting, and butterfly vibrations in the PCDD-OH adducts is negligible.

To further establish the well depth of DF-OH adducts, we have calculated the isodesmic reaction enthalpy for the formation of DF-OH(1) adducts by considering the isodesmic reaction: By using the experimental $\Delta_f H_{298}$ values for the cyclohexadienyl

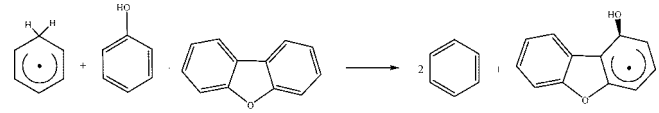

radical (50.6 ± 2.9 kcal/mol),[38] the phenol molecule (−23.0 kcal/mol),[39] dibenzofuran (11.3 kcal/mol),[39] and benzene (19.8 kcal/mol),[39] the heat of formation ($\Delta_f H_{298}$) for the DF-OH(1) adduct is calculated to be −0.4 ± 3.0 kcal/mol and the isodesmic well depth of enthalpy for the DF-OH(1) adduct is −20.6 ± 3.0 kcal/mol, compared to −18.8 kcal/mol calculated by using total energy differences. Thus, for the DF-OH adducts, the energetics obtained through the total energy differences are in reasonable agreement with the isodesmic reaction enthalpy. The difference between the two approaches might be within the accuracy of the isodesmic $\Delta_f H_{298}$, which depends on the choice of the isodesmic reaction scheme and the accuracy of $\Delta_f H_{298}$ of the reference compounds.

All OH addition reactions in Table 1, except DF + OH → DF-OH(B), are regarded as exothermic ($\Delta_r H_{298} < 0$), with no isomerization between the energized adducts, and thus, selectivity calculations based on kinetics derived by the activation barrier are more representative than predictions based on thermodynamic equilibrium product distribution. High-pressure limiting rate constants are based on the activation energies in Table 1 and listed in Table 4. The calculated rates for OH addition reactions are 1.5×10^{-11}, 3.1×10^{-12}, 6.1×10^{-12}, 1.9×10^{-13}, 4.3×10^{-15}, and 1.2×10^{-17} cm^3 $molecule^{-1}$ s^{-1} for sites C1−C4, C_A, and C_B, respectively, yielding an overall reaction rate constant for addition of OH of 2.4×10^{-11} cm^3 $molecule^{-1}$ s^{-1} (the reaction symmetry number is set to 2 in each case to match the possible optical isomers). In contrast, the rate constant calculated for H abstraction by OH at 298.15 K is 4.3×10^{-13} cm^3 $molecule^{-1}$ s^{-1} (the eight possible sites in the DF structure are considered for the reaction symmetry

SCHEME 2: Mechanistic Diagram of the DF-OH(1) Reaction with Dioxygen

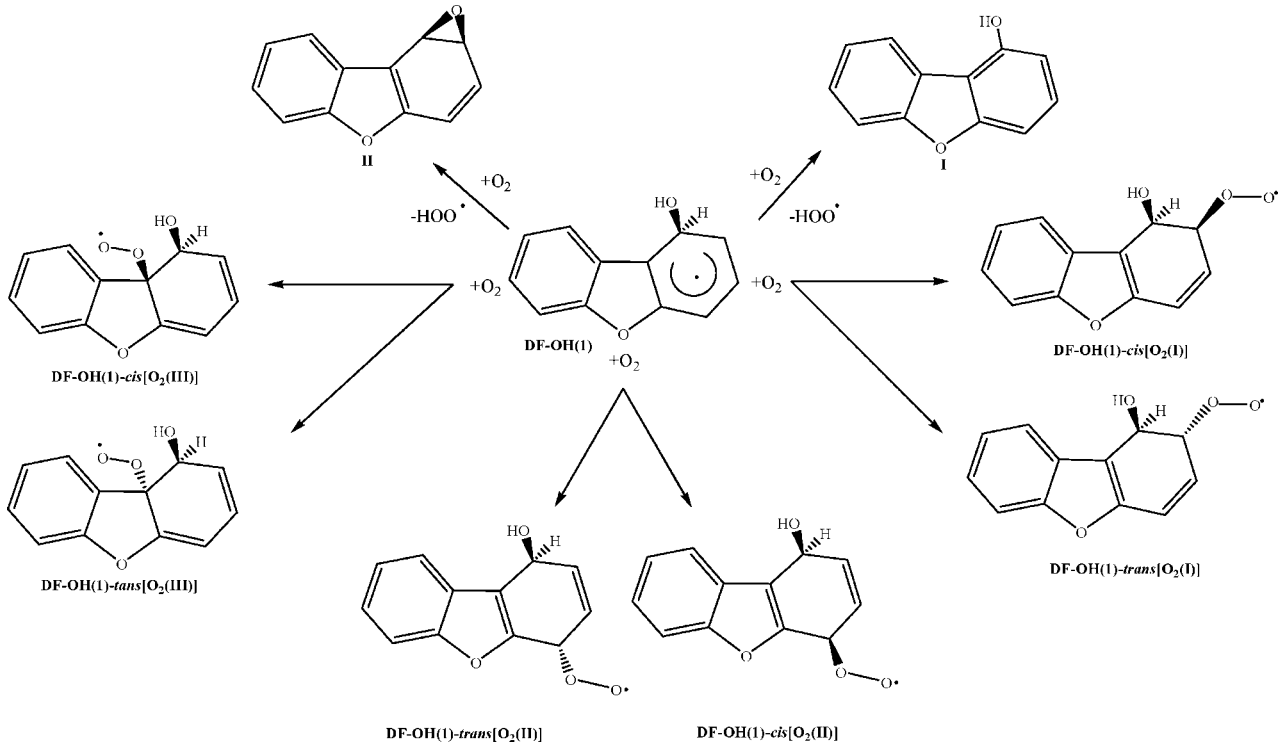

TABLE 1: B3LYP/6-311+G(3df,2p)//B3LYP/6-31G(d) Calculated Reaction Energies ($\Delta_r E°$), Activation Energies ($\Delta E^‡$) (at 0 K), Reaction Enthalpies ($\Delta_r H_{298}$), Activation Enthalpies ($\Delta H^‡$), Reaction Free Energies ($\Delta_r G_{298}$), and Free Energies of Activation ($\Delta G^‡$) (at 298.15 K and 1 atm) for OH Addition to DF[a]

reaction	$\Delta_r E_0$	$\Delta E^‡$	$\Delta_r H_{298}$	$\Delta H^‡$	$\Delta_r G_{298}$	$\Delta G^‡$
DF + OH → DF-OH(1)	−17.8	−2.1	−18.8	−2.8	−9.0	6.1
DF + OH → DF-OH(2)	−11.0	−1.4	−11.8	−2.1	−2.4	7.0
DF + OH → DF-OH(3)	−14.4	−1.7	−15.2	−2.4	−5.7	6.7
DF + OH → DF-OH(4)	−14.0	0.0	−14.9	−0.7	−5.3	8.2
DF + OH → DF-OH(A)	−12.6	2.0	−13.5	1.2	−3.5	10.6
DF + OH → DF-OH(B)	−1.5	5.1	−2.3	4.4	7.2	13.8

[a] All values are in kcal/mol.

TABLE 2: B3LYP/6-311+G(3df,2p)//B3LYP/6-31G(d) Energetics for the Reaction of O_2 with DF-OH(1) Adduct[a]

	reaction	$\Delta_r E_0$	$\Delta E^‡$	$\Delta_r H_{298}$	$\Delta H^‡$	$\Delta_r G_{298}$	$\Delta G^‡$
DF-OH(1) + O_2	DF-OH(1)-*cis*[O_2(I)]	−0.8	6.9	−1.6	6.5	10.0	16.3
	DF-OH(1)-*trans*[O_2(I)]	−1.4	6.7	−2.2	6.3	9.2	17.0
	DF-OH(1)-*cis*[O_2(II)]	−0.4	7.2	−1.0	6.7	9.8	16.3
	DF-OH(1)-*trans*[O_2(II)]	−0.5	6.9	−1.1	6.4	9.6	16.3
	DF-OH(1)-*cis*[O_2(III)]	10.7	12.9	9.8	12.1	21.8	23.6
	DF-OH(1)-*trans*[O_2(III)]	10.1	11.5	9.5	10.9	20.9	22.1

[a] All values are in kcal/mol.

TABLE 3: Energetics for the Individual Reactions in the Decomposition of DF-OH(1)

reaction	$\Delta_r E_0$	$\Delta E^‡$	$\Delta_r H_{298}$	$\Delta H^‡$	$\Delta_r G_{298}$	$\Delta G^‡$
DF-OH(1) + O_2 → I + HOO	−24.6	4.7	−23.6	4.1	−36.3	15.1
DF-OH(1) + O_2 → II + HOO	18.9	31.9	18.6	31.4	18.6	41.5

number). As the abstraction process involves an H movement, it is associated with a significant imaginary frequency (1463.8 cm^{-1}) and hence a large transmission coefficient. By including the transmission coefficient, the abstraction rate constant becomes 2.5×10^{-12} cm^3 $molecule^{-1}$ s^{-1}. The combined high-pressure limiting rate constant for abstraction and addition is 2.70×10^{-11} cm^3 $molecule^{-1}$ s^{-1} with the abstraction channel contributing 9.2% to the combined rate constant under the atmospheric conditions, a typical value for the contribution from the abstraction channel at atmospheric conditions. By assuming a 24 h average OH radical concentration of 9.7×10^5 molecule cm^{-3},[40] the lifetime of DF is determined to be 0.44 day. Atkinson[15] has determined the tropospheric lifetime of DF to be 1.7 and 3.1 days using the reaction rate constant determined by the structure−activity relationship (SAR)[41] and the experimental rate constant, respectively.

The calculated bimolecular rate constant for the reaction of DF + OH is 7 times faster than that obtained experimentally (3.9×10^{-12} cm^3 $molecule^{-1}$ s^{-1}) and within a factor of 4 of the theoretical value derived by Atkinson.[13,15] It is well-known

TABLE 4: High-Pressure Limit Rate Constant and Branching Ratios (*R*) of DF + OH Addition Reactions, and High-Pressure Limit Rate Constant for the Abstraction Reaction and the Overall Reactions (Addition + Abstraction)

species	k_{rec} (cm^3 $molecule^{-1}$ s^{-1})	*R*
DF-OH(1)	1.5×10^{-11}	0.61
DF-OH(2)	3.2×10^{-12}	0.13
DF-OH(3)	6.1×10^{-12}	0.25
DF-OH(4)	1.9×10^{-13}	8.2×10^{-3}
DF-OH(A)	4.3×10^{-15}	1.6×10^{-4}
DF-OH(B)	1.2×10^{-17}	7.7×10^{-7}
total addition	2.3×10^{-11}	
total abstraction	2.5×10^{-12}	
overall	2.7×10^{-11}	
predicted through SAR	7.0×10^{-12} [a]	
expt	3.9 (3.0−4.8) $\times 10^{-12}$ [b]	
	4.4×10^{-12} [c]	

[a] Reference 15. [b] Reference 13. [c] Reference 17.

that DFT simulations tend to underestimate activation barriers (see, e.g., ref 19), an observation which is consistent with this work. In our estimation of the rate constant by DFT, a statistical kinetic ordering was applied, based on activation energies presented in this study. The branching ratio (*R*) for OH addition reactions is reported in Table 4, based on the calculated high-pressure rate constant. These ratios are 0.61, 0.13, and 0.25 for DF-OH(1), DF-OH(2), and DF-OH(3), respectively, suggesting a strong preference for OH addition at site C1 while the addition of OH to the three other possible sites, C4, C_A, and C_B, are of minor importance in comparison.

Now we compare the kinetics for OH + DF with the experimental results obtained for other aromatic systems. The calculated rate constant for OH + DF is within a factor of 2 of the measured rate constant for OH + DD (dibenzo-*p*-dioxin; 4.58×10^{-11} cm^3 $molecule^{-1}$ s^{-1} [ref 36] and 1.2×10^{-11} cm^3 $molecule^{-1}$ s^{-1} [ref 13]) where a negative temperature dependence has also been observed. The calculated rate constant is almost 20 times faster than that for benzene,[19,37] 4 times faster than that of the toluene system,[38] only twice as fast as that of *p*-xylene,[23] and the same as that of phenol.[37] Thus, our calculated value for the rate constant for the OH + DF system is reasonably close to that of benzene-substituted systems (toluene, *p*-xylene, and phenol). An obvious explanation for the difference between OH addition to benzene and the benzene-substituted systems is that the substituent groups (CH_3 in toluene and OH in phenol) work as electron-releasing groups that facilitate the addition of OH to the aromatic system. In this regard, DF could also be considered to be a benzene-substituted system with the furan ring acting as the substituent group.

In Scheme 3, a direct dibenzofuran depletion mechanism is developed, which arises from the addition of OH to C_A and C_B in DF. Upon the addition of the OH to C_A, the adjacent C−O bond elongates by 0.078 Å, while the addition of OH to C_B elongates the adjacent C−C bond in the furan ring by 0.060 Å. Fission of the O−C bond in the DF-OH(A) structure produces the structure III, which is in a free energy well of 18.6 kcal/mol with respect to DF-OH(A), but its formation is impeded by a transition structure that is 12.8 kcal/mol above its entrance channel. The OH addition at the site C_B makes the rupture of the C−C bond in DF-OH(A) plausible in a process that forms structure IV. Formation of structure IV costs 9.6 kcal/mol of Gibbs free energy. Based on the branching ratio reported in Table 2, both reactions in Scheme 3 would be of little importance under atmospheric conditions, especially for the formation of structure IV from DF-OH(B), which has a free energy of activation of 28.3 kcal/mol. Their importance, however, may not be excluded at elevated temperatures where the entropy change with temperature would enhance the contribution of this reaction.

3.2. DF-OH Oxidation. According to Atkinson,[18] the hydroxycyclohexadienyl-type radical, which forms through the addition of OH to an aromatic benzene ring, is stabilized via collisions with the bath gas. Under atmospheric conditions, oxidation of benzene is initiated by OH, and a hydroxyl-2,4-cyclohexadienyl radical or benzene-OH adduct is formed and subsequently reacts with O_2.[20] Bimolecular modeling (QRRK) has established the formation of benzene−OH−O_2 as the dominant initial product which the flux of products, such as glyoxal ($(CHO)_2$) or methyl glyoxal (CH_3COCHO), go through. However, subsequent degradation mechanisms and the relationship of these pathways to the experimental results is not straightforward.[41] In this section, O_2 addition to the DF-OH(1) adduct is the most plausible adduct to result from OH addition to DF according to the branching ratio shown in Table 1. Additionally, H abstraction by O_2 from the hydroxyl group (OH) and H attached to H−C−OH are discussed in order to explore plausible channels for the reactions of O_2 with the most stable DF-OH adduct. These channels are displayed in Scheme 2.

Oxygen addition to the π-delocalized electron systems of the DF-OH(1) adducts occurs on the two carbon atoms *ortho* to the tetracoordinated carbon as well as to the *para* carbon, resulting in three distinguishable DF-OH-O_2 peroxy isomers for *cis* addition (with respect to the *ipso*-OH), denoted by DF-OH(1)-*cis*[O_2(I−III)], and three isomers for *trans* addition, denoted by DF-OH(1)-*trans*[O_2(I−III)]. These species, and their corresponding transition structures, are depicted in Figure 2. The energetics of these reactions are reported in Table 2. In the transition state structures, the double bond of O_2 is elongated by 0.03−0.04 Å while elongation in the resulting peroxy adducts ranges between 0.10 and 0.12 Å. Intermolecular hydrogen bonding between the lone pairs of the terminal oxygen atom of the peroxy group and the hydrogen of the hydroxyl group could exist in some isomers. Hydrogen bonding lengths range from 1.914 in the DF-OH(1)-*cis*[O_2(I)] isomer to 2.414 Å in the DF-OH(1)-*cis*[O_2(I)], with the latter values denoting a rather weak hydrogen association. This type of interaction also exists in some transition structures, especially in TS DF-OH(1)-*cis*[O_2(I)] where the intermolecular distance between the H of the attached hydroxyl group on site and the terminal oxygen atom is 1.902 Å. The transition vector corresponds to a single contribution characterized by the movement of the oxygen molecule toward the carbon atom involved in the bond.

The Gibbs free energies of activation ($\Delta G^{\ddagger}$) and activation energies ($\Delta E^{\ddagger}$) range from 16.3 and 6.7 kcal/mol to 23.6 and 12.9 kcal/mol, respectively. As Table 2 shows, O_2 addition in either *cis* or *trans* orientation is preferred on sites I and II. In fact, the small difference in energetics data reported for the four DF-OH(1)-O_2 isomers in sites I and II is most likely to be within the accuracy limits of the computational approach. For bimolecular reactions, an increase in the Gibbs free energy of activation compared to the energy and enthalpies of activation is expected. This is compared with 3.8 kcal/mol based on a DFT calculated activation energy for O_2 addition to the benzene-OH adduct,[20] 6.5 kcal/mol for the *m*-xylene-OH adduct,[24] 8.6 kcal/mol for the toluene-OH adduct,[24] and 5.0 kcal/mol for *p*-xylene.[20]

As shown in Table 2, the formation of the six isomers is nonspontaneous, and most isomers are modestly stable and are

SCHEME 3: Central Bond Scission upon Addition of OH to C_A and C_B

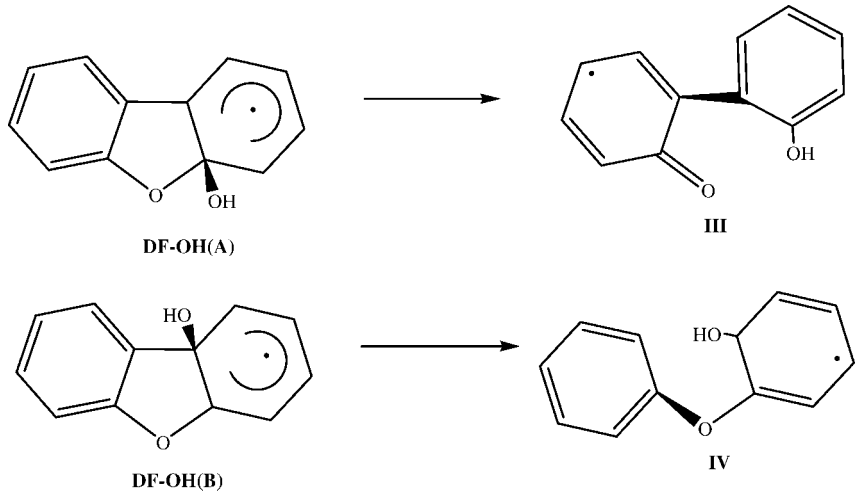

higher in energy/enthalpy than their corresponding separated reactants (O_2 and DF-OH adducts).

3.3. Formation of Dibenzofuranol. Phenol is the major product of benzene oxidation under atmospheric conditions.[15,39–42]

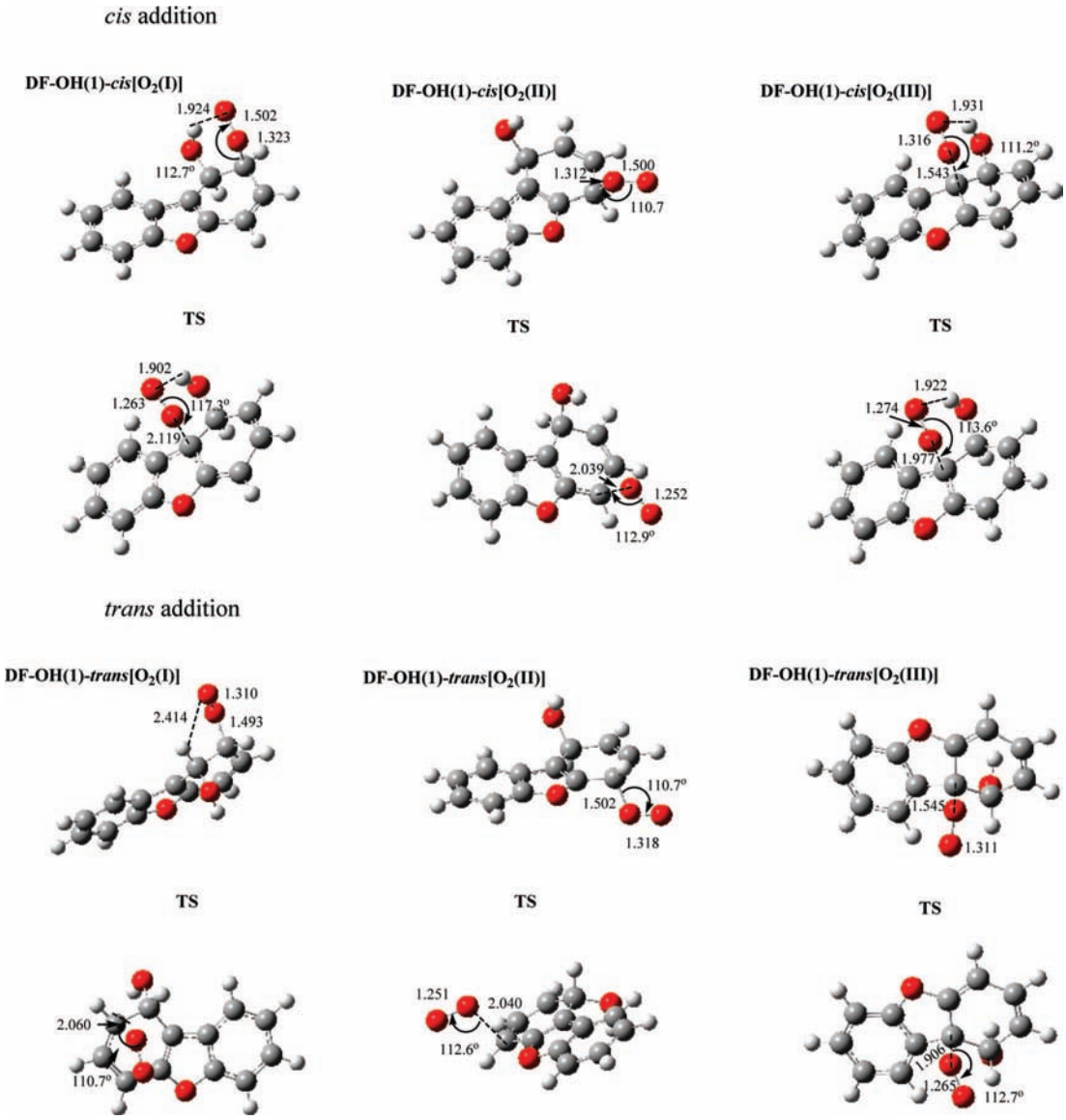

Figure 2. Optimized geometries for DF-OH-O_2 adducts and their corresponding transition structures (interatomic distances in angstroms, and angles in degrees).

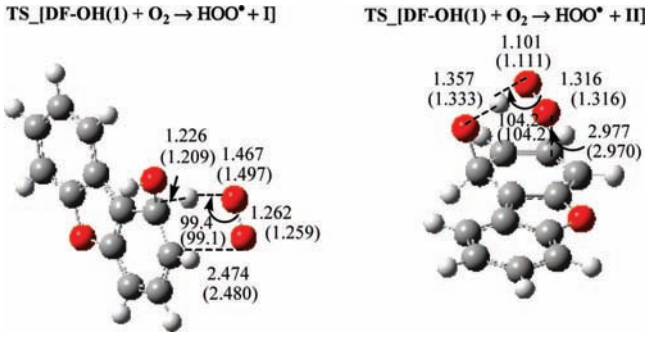

Figure 3. Optimized geometries of transition structures of the formation of structures I and II at the B3LYP/6-31G(d) level of theory; values in the brackets were obtained with the basis set of 6-31G(d,p).

The yield of phenol in the these studies ranges from 23 to 53%, based on the initial reaction conditions. It is shown that phenol production arises from the reaction of an oxygen molecule with a benzene-OH adduct and not from the photolysis of oxide/oxepin of benzene.[41] Theoretically,[20] an oxygen molecule abstracts H *gem* to OH, affording phenol through a barrier of only 2.8 kcal/mol at 298 K in a reaction that generates 27.1 kcal/mol and the products HOO and phenol. By analogy, we examine the reaction between an oxygen molecule and the DF-OH(1) adduct to produce dibenzofuranol. In Scheme 2, an oxygen molecule abstracts H *gem* to OH at site C1 and produces 1-dibenzofuranol (I). The most important optimum geometrical parameters for the transition structure are shown in TS_[DF-OH(1) + O_2 → HOO + I] of Figure 3. The free energy of activation of this reaction is 15.1 kcal/mol, while the activation energy (at 0 K) is 4.7 kcal/mol. The reaction is exergonic by 36.3 kcal/mol ($\Delta_r G_{298}$) under atmospheric conditions and exothermic by 23.6 kcal/mol ($\Delta_r H_{298}$). With respect to the other reactions presented in Scheme 2, as hydroxyl hydrogen is abstracted by an oxygen molecule, the free oxygen bends toward C2 in a concerted process, resulting in the formation of an epoxide structure (II) through transition state TS_[DF-OH(1) + O_2 → HOO + II], as displayed in Figure 3. The free energy of activation for this reaction is calculated to be 41.5 kcal/mol, which indicates that it would not contribute significantly to DF decomposition under atmospheric reaction conditions. Note that I and II are stable products that could be detected experimentally. Since the last two reactions involve H movement, we have also located their transition structures with the basis set of 6-31G(d,p) and the comparison in geometries is shown in Figure 3 where only small differences are obtained. In terms of energetics, the activation energies increase by only 0.2 kcal/mol for TS_[DF-OH(1) + O2 → HOO + I] and by only 0.1 kcal/mol for TS_[DF-OH(1) + O2 → HOO + II].

The branching ratio between dioxygen addition to the π-delocalized system (at three possible sites I, II, and III) of DF-OH(1) and H abstraction (mainly H in the tetracoordinated carbon to afford I) is detetermined based on the high-pressure rate constant (k_∞) tabulated in Table 5. The combined k_∞ value for the addition reaction is 3.4×10^{-19} cm^3 molecule^{-1} s^{-1} (producing mainly DF-OH(1)-*cis*[O_2(II)] with a selectivity of 76% and DF-OH(1)-*trans*[O_2(I)] with a selectivity of 24%) compared with 1.5×10^{-18} cm^3 molecule^{-1} s^{-1} for the production of I. Dioxygen addition reactions will then lead to ring fragmentation, while production of I retains the ring structure (ring retention). The branching ratio for the formation of I (83%) is higher than the percentage yield of 23−53% measured experimentally for the formation of phenol from atmospheric oxidation of benzene.[15,41–44] A study on the fate of the DF-OH(1)-*cis*[O_2(II)] adduct, since it is the DF-OH(1)-O_2 adduct with the highest formation ratio, will be carried out in due course.

TABLE 5: High-Pressure Limit Rate Constant for O_2 Reaction with DF-OH(1) under Atmospheric Conditions

reaction		k_{rec} (cm^3 molecule^{-1} s^{-1})
DF-OH(1) + O_2 →	(1) DF-OH(1)-*cis*[O_2(I)]	4.5×10^{-20}
	(2) DF-OH(1)-*trans*[O_2(I)]	7.6×10^{-20}
	(3) DF-OH(1)-*cis*[O_2(II)]	2.3×10^{-19}
	(4) DF-OH(1)-*trans*[O_2(II)]	1.4×10^{-19}
	(5) DF-OH(1)-*cis*[O_2(III)]	1.0×10^{-24}
	(6) DF-OH(1)-*trans*[O_2(III)]	1.3×10^{-23}
	total (2 + 3 + 6)	3.1×10^{-19}
DF-OH(1) + O_2 → I + HOO		1.5×10^{-18}
DF-OH(1) + O_2 → II + HOO		1.7×10^{-37}

4. Conclusions

An investigation, based on DFT calculations, was undertaken to elucidate the mechanistic features of OH-initiated oxidation reactions of dibenzofuran (DF). Reactants, products, and transition structures have been determined for the initial decomposition channels. The most dominant pathways taking place under atmospheric conditions have been determined by comparing reaction rate constants. Addition of OH to DF produces six different DF-OH adducts and occurs predominantly at sites C1, C2, and C3 with a selectivity of 0.61 on site C1. For the initial oxidation steps, ring retention reactions affording dibenzofuranol formation dominate oxygen addition reactions, which most likely lead to ring fragmentation.

Acknowledgment. This research has been supported by a grant from the Australian Research Council. M.A. acknowledges the award of a postgraduate studentship by the Al-Hussein Bin Talal University (Jordan). The authors acknowledge the access to the computational facilities of the Australian Centre of Advanced Computing and Communications (ac3).

Supporting Information Available: Calculated total energies, zero point energies, Cartesian coordinates, moments of inertia, and vibrational frequencies of all equilibrium and transition states structures. This material is available free of charge via the Internet at http://pubs.acs.org.

References and Notes

(1) Lin, L.-F. L. Wen-Jhy; Chang-Chien, Guo-Ping. *J. Air Waste Manage. Assoc.* **2006**, *6*, 1707.
(2) Baker, J. I.; Hites, R. A. *Environ. Sci. Technol.* **2000**, *34*, 2879.
(3) Fox, J. L. *Science* **1983**, *221*, 1161.
(4) Li, Q.; Qing; Loganath, A.; Chong, Y.; SengTan, J. O.; Jeffrey, P. *J. Toxicol. Environ. Health, Part A* **2006**, *69*, 1987.
(5) Lohmann, R.; Ockenden, W. A.; Shears, J.; Jones, K. C. *Environ. Sci. Technol.* **2001**, *35*, 4046.
(6) Panshin, S. Y.; Hites, R. A. *Environ. Sci. Technol.* **1994**, *28*, 2008.
(7) Tysklind, M.; Faengmark, I.; Marklund, S.; Lindskog, A.; Thaning, L.; Rappe, C. *Environ. Sci. Technol.* **1993**, *27*, 2190.
(8) Broman, D.; Naef, C.; Zebuehr, Y. *Environ. Sci. Technol.* **1991**, *25*, 1841.
(9) Rordorf, B. F. *Chemosphere* **1989**, *18*, 783.
(10) Bidleman, T. F. *Environ. Sci. Technol.* **1988**, *22*, 361.
(11) Manchester-Neesvig, J. B.; Andren, A. W. *Environ. Sci. Technol.* **1989**, *23*, 1138.
(12) Ballschmiter, K.; Wittlinger, R. *Environ. Sci. Technol.* **1991**, *25*, 1103.
(13) Kwok, E. S. C.; Arey, J.; Atkinson, R. *Environ. Sci. Technol.* **1994**, *28*, 528.
(14) Addink, R.; Olie, K. *Environ. Sci. Technol.* **1995**, *29*, 1425.

(15) Atkinson, R. Atmospheric Chemistry of PCBs, PCDDs and PCDFs. In *Issues in Environmental Science and Technology*; Hester, R. E., Harrison, R. M., Eds.; 1996; Vol. 6, p 53.
(16) Brubaker, W. W.; Hites, R. A. *Environ. Sci. Technol.* **1997**, *31*, 1805.
(17) Brubaker, W. W.; Hites, R. A. *J. Phys. Chem. A* **1998**, *102*, 915.
(18) Atkinson, R. *J. Phys. Chem. Ref. Data, Monogr.* **1989**, *1*, 1.
(19) Lay, T. H.; Bozzelli, J. W.; Seinfeld, J. H. *J. Phys. Chem.* **1996**, *100*, 6543.
(20) Ghigo, G.; Tonachini, G. *J. Am. Chem. Soc.* **1998**, *120*, 6753.
(21) Uc, V. H.; Garcia-Cruz, I.; Hernandez-Laguna, A.; Vivier-Bunge, A. *J. Phys. Chem. A* **2000**, *104*, 7847.
(22) García-Cruz, I.; Miguel Castro, M.; Vivier-Bunge, A. *J. Comput. Chem.* **2000**, *21*, 716.
(23) Fan, J.; Zhang, R. *J. Phys. Chem. A* **2006**, *110*, 7728.
(24) Andino, J. M.; Smith, J. N.; Flagan, R. C.; Goddard, W. A.; Seinfeld, J. H. *J. Phys. Chem.* **1996**, *100*, 10967.
(25) Lee, J. E.; Choi, W.; Mhin, B. J.; Balasubramanian, K. *J. Phys. Chem. A* **2004**, *108*, 607.
(26) Frisch, M. J.; Trucks, G. W.; Schlegel, H. B.; Scuseria, G. E.; Robb, M. A.; Cheeseman, J. R.; Zakrzewski, V. G.; Montgomery, J. A.; Stratmann, R. E.; Burant, J. C.; Dapprich, S.; Millam, J. M.; Daniels, R. E.; Kudin, K. N.; Strain, M. C.; Farkas, O.; Tomasi, J.; Barone, V. C.M.; Cammi, R.; Mennucci, B.; Pomelli, C.; Adamo, C.; Clifford, S.; Ochterski, J.; Petersson, G. A.; Ayala, P. Y.; Cui, Q.; Morokuma, K.; Salvador, P.; Dannenberg, J. J.; Malick, D. K.; Rabuck, A. D.; Raghavachari, K.; Foresman, J. B.; Cioslowski, J. O. J.V.; Baboul, A. G.; Stefanov, B. B.; Liu, G.; Liashenko, A.; Piskorz, P.; Komaromi, I.; Gomperts, R.; Martin, R. L.; Fox, D. J.; Keith, T.; Al-Laham, M. A.; Peng, C. Y.; Nanayakkara, A.; Challacombe, M.; Gill, P. M. W.; Johnson, B.; Chen, W.; Wong, M. W.; Andres, J. L.; Gonzalez, C. M.; Head-Gordon, M.; Replogle, E. S.; Pople, J. A. *Gaussian 03*, revision A.11; Gaussian, Inc.: Pittsburgh, PA, 2001.
(27) Becke, A. D. *J. Chem. Phys.* **1993**, *98*, 5648.
(28) Lee, C.; Yang, W.; Parr, R. G. *Phys. Rev. B.* **1988**, *37*, 785.
(29) Montgomery, J. J. A.; Ochterski, J. W.; Petersson, G. A. *J. Chem. Phys.* **1994**, *101*, 5900.
(30) Altarawneh, M.; Dlugogorski, B. Z.; Kennedy, E. M.; Mackie, J. C. *J. Phys. Chem. A* **2006**, *110*, 13560.
(31) McQuarrie, D. A. *Statistical Mechanics*; Harper Collins: New York, 1976.
(32) Eckart, C. *Phys. Rev.* **1930**, *35*, 1303.
(33) Duncan, W. T.; Bell, R. L.; Truong, T. N. *J. Comput. Chem.* **1998**, *19*, 1039.
(34) Tokmakov, I. V.; Lin, M. C. *J. Phys. Chem. A* **2002**, *106*, 11309.
(35) Chen, C.-C.; Bozzelli, J. W.; Farrell, J. T. *J. Phys. Chem. A* **2004**, *108*, 4632.
(36) Taylor, P. H.; Yamada, T.; Neuforth, A. *Chemosphere* **2005**, *58*, 243.
(37) Knispel, R.; Koch, R.; Siese, M.; Zetzsch, C. *Ber. Bunsen−Ges.* **1990**, *94*, 1375.
(38) Berho, F.; Rayez, M.; Lesclaux, R. *J. Phys. Chem. A* **1999**, *103*, 5501.
(39) Afeefy, H. Y.; Liebman, J. F.; Stein, S. E. Neutral Thermochemical Data. In *NIST Chemistry WebBook, NIST Standard Reference Database Number 69*; Linstrom, P. J., Mallard, W. G., Eds.; National Institute of Standards and Technology: Gaithersburg, MD, 2005; http://webbook.nist-.gov.
(40) Bohn, B. *J. Phys. Chem. A* **2001**, *105*, 6092.
(41) Volkamer, R.; Klotz, B.; Barnes, I.; Imamura, T.; Wirtz, K.; Washida, N.; Becker, K. H.; Platt, U. *Phys. Chem. Chem. Phys.* **2002**, *4*, 1598.
(42) Atkinson, R.; Aschmann, S. M.; Arey, J.; Carter, W. P. L. *Int. J. Chem. Kinet.* **1989**, *21*, 801.
(43) Bjergbakke, E.; Sillesen, A.; Pagsberg, P. *J. Phys. Chem.* **1996**, *100*, 5729.
(44) Klotz, B.; Barns, I.; Becker, K. H.; Golding, B. T. *J. Chem. Soc., Faraday Trans.* **1997**, *93*, 1507.

JP800093J